



AFRL-AFOSR-VA-TR-2016-0331

Optimized Routing of Intelligent, Mobile Sensors for Dynamic,
Data-Driven Sampling

**Derek Paley
MARYLAND UNIV COLLEGE PARK
3112 LEE BLDG
COLLEGE PARK, MD 20742 - 5100**

**09/27/2016
Final Report**

DISTRIBUTION A: Distribution approved for public release.

Air Force Research Laboratory
AF Office Of Scientific Research (AFOSR)/RTA2

REPORT DOCUMENTATION PAGEForm Approved
OMB No. 0704-0188

The public reporting burden for this collection of information is estimated to average 1 hour per response, including the time for reviewing instructions, searching existing data sources, gathering and maintaining the data needed, and completing and reviewing the collection of information. Send comments regarding this burden estimate or any other aspect of this collection of information, including suggestions for reducing the burden, to the Department of Defense, Executive Service Directorate (0704-0188). Respondents should be aware that notwithstanding any other provision of law, no person shall be subject to any penalty for failing to comply with a collection of information if it does not display a currently valid OMB control number.

PLEASE DO NOT RETURN YOUR FORM TO THE ABOVE ORGANIZATION.

1. REPORT DATE (DD-MM-YYYY)	2. REPORT TYPE	3. DATES COVERED (From - To)		
4. TITLE AND SUBTITLE			5a. CONTRACT NUMBER	
			5b. GRANT NUMBER	
			5c. PROGRAM ELEMENT NUMBER	
6. AUTHOR(S)			5d. PROJECT NUMBER	
			5e. TASK NUMBER	
			5f. WORK UNIT NUMBER	
7. PERFORMING ORGANIZATION NAME(S) AND ADDRESS(ES)			8. PERFORMING ORGANIZATION REPORT NUMBER	
9. SPONSORING/MONITORING AGENCY NAME(S) AND ADDRESS(ES)			10. SPONSOR/MONITOR'S ACRONYM(S)	
			11. SPONSOR/MONITOR'S REPORT NUMBER(S)	
12. DISTRIBUTION/AVAILABILITY STATEMENT DISTRIBUTION A: Distribution approved for public release.				
13. SUPPLEMENTARY NOTES				
14. ABSTRACT				
15. SUBJECT TERMS				
16. SECURITY CLASSIFICATION OF: a. REPORT b. ABSTRACT c. THIS PAGE		17. LIMITATION OF ABSTRACT	18. NUMBER OF PAGES	19a. NAME OF RESPONSIBLE PERSON 19b. TELEPHONE NUMBER (Include area code)

INSTRUCTIONS FOR COMPLETING SF 298

- 1. REPORT DATE.** Full publication date, including day, month, if available. Must cite at least the year and be Year 2000 compliant, e.g. 30-06-1998; xx-06-1998; xx-xx-1998.
- 2. REPORT TYPE.** State the type of report, such as final, technical, interim, memorandum, master's thesis, progress, quarterly, research, special, group study, etc.
- 3. DATES COVERED.** Indicate the time during which the work was performed and the report was written, e.g., Jun 1997 - Jun 1998; 1-10 Jun 1996; May - Nov 1998; Nov 1998.
- 4. TITLE.** Enter title and subtitle with volume number and part number, if applicable. On classified documents, enter the title classification in parentheses.
- 5a. CONTRACT NUMBER.** Enter all contract numbers as they appear in the report, e.g. F33615-86-C-5169.
- 5b. GRANT NUMBER.** Enter all grant numbers as they appear in the report, e.g. AFOSR-82-1234.
- 5c. PROGRAM ELEMENT NUMBER.** Enter all program element numbers as they appear in the report, e.g. 61101A.
- 5d. PROJECT NUMBER.** Enter all project numbers as they appear in the report, e.g. 1F665702D1257; ILIR.
- 5e. TASK NUMBER.** Enter all task numbers as they appear in the report, e.g. 05; RF0330201; T4112.
- 5f. WORK UNIT NUMBER.** Enter all work unit numbers as they appear in the report, e.g. 001; AFAPL30480105.
- 6. AUTHOR(S).** Enter name(s) of person(s) responsible for writing the report, performing the research, or credited with the content of the report. The form of entry is the last name, first name, middle initial, and additional qualifiers separated by commas, e.g. Smith, Richard, J, Jr.
- 7. PERFORMING ORGANIZATION NAME(S) AND ADDRESS(ES).** Self-explanatory.
- 8. PERFORMING ORGANIZATION REPORT NUMBER.** Enter all unique alphanumeric report numbers assigned by the performing organization, e.g. BRL-1234; AFWL-TR-85-4017-Vol-21-PT-2.
- 9. SPONSORING/MONITORING AGENCY NAME(S) AND ADDRESS(ES).** Enter the name and address of the organization(s) financially responsible for and monitoring the work.
- 10. SPONSOR/MONITOR'S ACRONYM(S).** Enter, if available, e.g. BRL, ARDEC, NADC.
- 11. SPONSOR/MONITOR'S REPORT NUMBER(S).** Enter report number as assigned by the sponsoring/monitoring agency, if available, e.g. BRL-TR-829; -215.
- 12. DISTRIBUTION/AVAILABILITY STATEMENT.** Use agency-mandated availability statements to indicate the public availability or distribution limitations of the report. If additional limitations/ restrictions or special markings are indicated, follow agency authorization procedures, e.g. RD/FRD, PROPIN, ITAR, etc. Include copyright information.
- 13. SUPPLEMENTARY NOTES.** Enter information not included elsewhere such as: prepared in cooperation with; translation of; report supersedes; old edition number, etc.
- 14. ABSTRACT.** A brief (approximately 200 words) factual summary of the most significant information.
- 15. SUBJECT TERMS.** Key words or phrases identifying major concepts in the report.
- 16. SECURITY CLASSIFICATION.** Enter security classification in accordance with security classification regulations, e.g. U, C, S, etc. If this form contains classified information, stamp classification level on the top and bottom of this page.
- 17. LIMITATION OF ABSTRACT.** This block must be completed to assign a distribution limitation to the abstract. Enter UU (Unclassified Unlimited) or SAR (Same as Report). An entry in this block is necessary if the abstract is to be limited.

Optimized Routing of Intelligent, Mobile Sensors for Dynamic, Data-Driven Sampling

Derek A. Paley

Abstract The report describes a Dynamic Data-Driven Application Systems (DDDAS) project in which multiple mobile sensors are routed via a data-driven sampling scheme. The long-term goal of this project is to provide a control-theoretic framework to enable intelligent, mobile systems to optimally collect sensor-based observations that yield accurate estimates of unknown processes such as aircraft formation flight and environmental monitoring. The basic research objective is to apply tools from aerospace engineering, specifically nonlinear estimation and control, to design coordinated sampling trajectories that yield the most informative measurements of estimated dynamical and stochastic systems. The technical approach to achieve this objective is to construct a framework for dynamic, data-driven sampling algorithms that (1) maximize the observability of a nonlinear dynamical system subject to time-varying perturbations; and (2) minimize the uncertainty in the estimate of a nonstationary random process that requires nonuniform sampling. The approach incorporates complementary representations of an unknown process: the first uses a deterministic, model-based parametrization, whereas the second uses a low-dimensional statistical description; both approaches apply and enable the DDDAS concept in which measurement data is used to update the model description and the updated model is used to guide subsequent measurements.

1 Introduction

Observability-based optimization in path planning [74] and data assimilation [38] typically uses either a low-dimensional parameterized model or an empirical data-based representation of the unknown process; however, problems arise when neither a suitable model nor sufficient data are available. The novelty of the approach described in this report lies in the study of the observability of a low-

Derek A. Paley
University of Maryland, College Park, MD, e-mail: dpaley@umd.edu

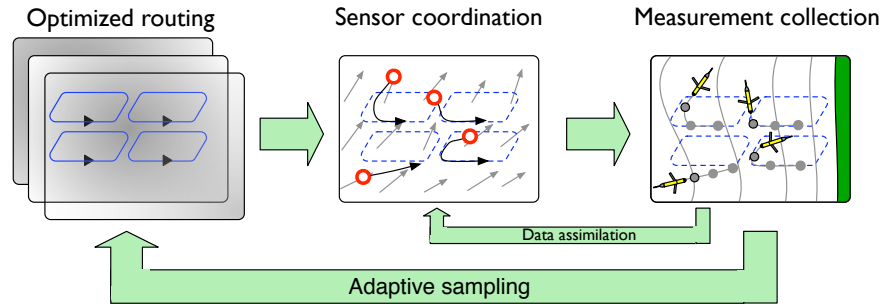


Fig. 1 The DDDAS framework for dynamic, data-driven sampling uses (left) information-based metrics to optimize sensor routes, (middle) multi-vehicle control to stabilize the desired trajectories, and (right) nonlinear filtering to assimilate data; adaptive sampling refers to the re-optimization of sensor routes that occurs after data assimilation.

dimensional model of an environmental vector field and the use of the output of a data-assimilation filter to guide the observability analysis via metrics from Bayesian experimental design. Observability- and information-based optimization of sampling trajectories has the potential to yield a reliable and predictable capability for intelligent, mobile sensors under the Dynamic Data-Driven Application Systems (DDDAS) concept. Dynamic, data-driven Bayesian nonlinear filtering can exploit noisy, low-fidelity and nonlinear measurements collected in a distributed manner either onboard a single sensor platform or by multiple sampling platforms.

Although methods exist for the optimization of sampling trajectories using distributed parameter estimation [17], optimal interpolation [44], and heuristic approaches [67], an open question is how to rigorously characterize the variability of information content in the unknown process and how to target observations in the information-rich regions. The merit of the approach described in this report lies in the design of a statistical framework based on spatiotemporal estimation of nonstationary processes in meteorology [35] and geostatistics [33], and the use of this framework to employ the DDDAS concept for sampling environmental fields. The framework extends the authors' previous work in this area into multiple dimensions and incorporates the challenge of building a nonstationary statistical representation of a random process while simultaneously optimizing the sampling trajectories. Figure 1 summarizes the overall workflow for data-driven routing of mobile sensor platforms.

The power of a DDDAS-based approach to sampling optimization is demonstrated by its ubiquity in fields ranging from robots for environmental monitoring and spatial estimation [19, 24, 12, 3, 75, 20] to atmospheric science and hurricane research [59, 8, 7, 48, 42]. One field that has particularly advanced the DDDAS framework is oceanography [2, 23, 15, 49, 66, 73, 29, 45, 6], in which autonomous underwater vehicles are used as mobile sensors for adaptive sampling. Indeed the concept of optimal experimental design was first applied to oceanographic sampling in the 1980's [5]. The optimization of sensor placement and data collection has ap-

plications in fighting wildfires [39], finding perturbation sources in power networks [11], and in spatial data collection for geostatistics [52, 70]. Perhaps it is not surprising, given to the range of these applications, that there are a variety of approaches advocated in the literature, including adaptation based on maximum *a posteriori* estimation [72]; stochastic deployment policies [50, 51]; information-based methods [34, 1, 26]; learning and artificial intelligence [63, 62, 14]; deterministic methods with heuristic metrics [69, 65]; bio-inspired source localization and gradient climbing [25, 27]; and nonparametric Bayesian models [10]. The results described in this report differ from prior work on adaptive sampling of dynamical systems [13] and random processes [4, 12], in the novel application of nonlinear observability and control coupled with recursive Bayesian filtering to optimize sensor routing for environmental sampling.

Observability in control theory is a measure of how well the state variables of a system can be determined by measurements of its outputs. Observability of a linear system is well studied [32] and is characterized using the Kalman rank condition, which is a special case of the observability rank condition of a general, nonlinear system [31]. A nonlinear system is called *observable* if two states are indistinguishable only if the states are identical [31]. Observability in data assimilation refers to the ability to determine the parameters of an unknown process by using a time history of observations [37]. Although standard observability tests give a binary answer (observable or not), the degree of observability can be computed from the singular values of the observability gramian [38], which is a Hermitian matrix of inner products of the system's outputs. Computation of the empirical observability gramian [40] requires only the ability to simulate the system, and is therefore particularly attractive for numerical optimization. Algorithms for observability-based estimation and path planning have broader applications in satellite control [47] and micro air vehicles [74].

Optimal statistical interpolation of sensor observations to produce a stochastic estimate of an unknown random process is based on classical estimation theory [46], and is formerly known in meteorology and oceanography as objective analysis [9]. Optimal interpolation also yields a measure of the uncertainty or error in the estimate, which can be used as a measure of estimator performance or skill [16]. It is common to compute estimator error under the assumption of stationarity of the spatial and temporal variability of the unknown process [44], although these assumptions may not be borne out in applications of interest. A stochastic process whose variability changes when shifted in time or space is called *nonstationary* [60, 56], and methods exist to parametrize nonstationary processes in oceanography [68, 35] and geostatistics [33, 57, 71]. Indeed, nonstationary-based strategies have been previously applied to mobile sensor networks [72], though not based on a principled control design as described here.

The remainder of the report is organized as follows. Section 2 provides an overview of two complementary approaches to data-driven adaptive sampling. Section 3 summarizes an application example of observability-based sensor routing for aircraft proximity flight as first presented in [43]. Section 4 reviews an application

example of coverage control of a nonstationary spatiotemporal field following [54]. Section 5 summarizes the report and ongoing research.

2 Data-driven Adaptive Sampling

2.1 Measures of Observability

Successful estimation of states in a system depends on the ability to observe the desired states from the sensor measurements collected over time [38]. For instance, in the application example considered in Section 3, one seeks to observe the wake parameter states of an aircraft given measurements of the differential pressure coefficients along the wing of a second aircraft. This section provides a brief overview of observability in the context of linear and nonlinear systems and reviews the empirical observability gramian [41, 38] used to assess the observability of the wake parameters in the aerodynamic model described in Section 3.

A dynamical system is said to be observable if its initial conditions can be determined from a time history of output measurements and control inputs over some time interval [31, 64]. A standard method of measuring observability is to calculate the singular values of the observability gramian [64]. In linear systems theory, the singular values of the observability gramian quantify the ease in determining the initial states from the outputs generated over time as follows: large singular values imply the mapping is easily invertible, whereas small or zero singular values imply it is not [64, p.125–126]. This report quantifies the unobservability of a system using the unobservability index ξ , which is the reciprocal of the smallest singular value σ_{min} , i.e., [38]

$$\xi = \frac{1}{\sigma_{min}}. \quad (1)$$

The unobservability index (1) reflects the least observable mode in the system and provides a worst-case observability measure for the system.

The observability of a nonlinear system may be difficult to determine analytically, because it requires tools from differential geometry [31]. If the dynamical model of interest is solved numerically, it is justified to pursue numerical techniques for calculating the nonlinear, empirical observability gramian [38, 28]. The empirical observability gramian does not require linearization, which may fail to adequately model the input/output relationship of the nonlinear system over a wide range of operating conditions, but merely the ability to simulate the system [38]. Indeed, the empirical observability gramian maps the input-output behavior of a nonlinear system more accurately than the observability gramian produced by linearization of the nonlinear system [28]. The empirical observability gramian is a square matrix whose dimension matches the size of the state vector and whose i, j th entry represent the sensitivity of the output to infinitesimal perturbations about their nominal value of the corresponding i and j states or unknown parameters.

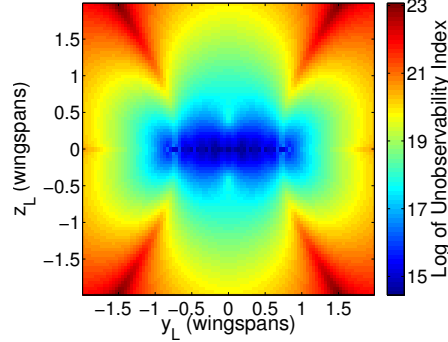


Fig. 2 The log of the unobservability index of an aircraft wake over a range of relative positions of a follower aircraft equipped with distributed pressure sensors. Reprinted from [43] with permission from the American Institute of Aeronautics and Astronautics.

The empirical observability gramian is formally defined as follows. Let $\varepsilon_i \mathbf{e}_i$, $i = 1, \dots, M$, be a small displacement of the nominal parameter along the i th unit vector $\mathbf{e}_i \in \mathbb{R}^M$ and let $\boldsymbol{\Omega} \in \mathbb{R}^M$ be the set of nominal parameter values. The $(i, j)^{\text{th}}$ component of the $M \times M$ empirical observability gramian W_O is [38]

$$W_O(i, j) = \frac{1}{4\varepsilon_i \varepsilon_j} \int_0^T [\boldsymbol{\phi}^{+i}(\tau) - \boldsymbol{\phi}^{-i}(\tau)]^T [\boldsymbol{\phi}^{+j}(\tau) - \boldsymbol{\phi}^{-j}(\tau)] d\tau, \quad (2)$$

$$i = 1, \dots, M, \quad j = 1, \dots, M,$$

where $\boldsymbol{\Omega}^{\pm i} = \boldsymbol{\Omega} \pm \varepsilon_i \mathbf{e}_i$ produces the output $\boldsymbol{\phi}^{\pm i} = \mathbf{h}(\boldsymbol{\Omega}^{\pm i}, \mathbf{u})$. The observability of a nonlinear system is measured by calculating the unobservability index (1) of the empirical observability gramian W_O .

Figure 2 depicts the observability of an aircraft wake in a plane orthogonal to a follower aircraft, revealing blind spots in which the follower aircraft may not be able to detect the leader's wake. Evaluation of the empirical observability gramian over the space of leader aircraft positions provides an observability map of the leader aircraft wake (see Section 3 for model details). The observability analysis is used in Section 3 to guide the design of a recursive Bayesian filter for estimating the leader's wake parameters and an observability-based control strategy to steer the follower to a desired relative position. Maintaining adequate observability along the trajectory guarantees the performance of the filtering scheme.

2.2 Evaluating Mapping Error

A spatiotemporal field is statistically described by its mean and the covariance function between any two points i and j . A covariance function is a positive-definite function that describes the variability of the field between the i th and j th location, as described in [6]. A field is stationary if its covariance function depends

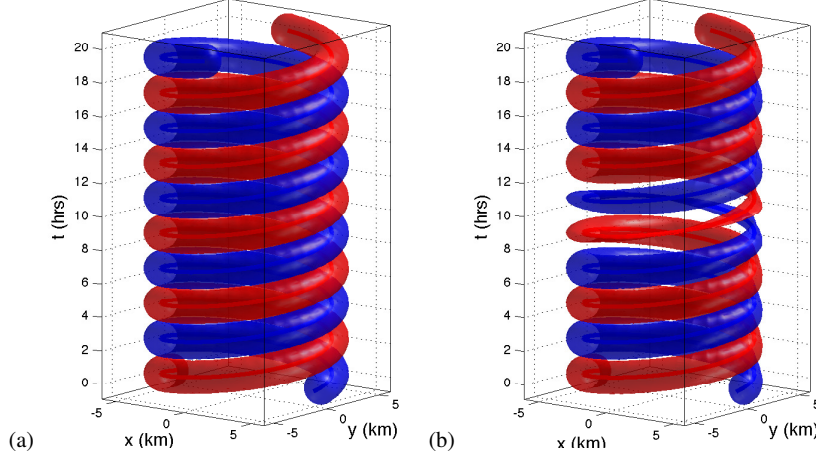


Fig. 3 Two vehicles traveling through (a) stationary and (b) nonstationary spatiotemporal fields. The tubes represent the volume covered by sensor measurements. Reprinted from [54] with permission from Elsevier.

only on the relative position of i and j and is nonstationary if it depends on i and j independently. There are a number of choices for the form of a nonstationary covariance function, e.g., Matern, rational quadratic, Ornstein-Uhlenbeck and squared-exponential forms as described in [33]. For the statistics-based sampling strategy described in Section 4, we require a covariance function that is a product of a spatial covariance function and a temporal covariance function.

To represent spatiotemporal fields with non-uniform coverage requirements, we adopt a nonstationary squared exponential covariance function of the following form, as introduced in [33]:

$$C(r_i, r_j) = \frac{|\Sigma(r_i)|^{1/4} |\Sigma(r_j)|^{1/4}}{\left| \frac{\Sigma(r_i) + \Sigma(r_j)}{2} \right|^{1/2}} \exp \left[-\frac{1}{2} (r_i - r_j)^T \left(\frac{\Sigma(r_i) + \Sigma(r_j)}{2} \right)^{-1} (r_i - r_j) \right], \quad (3)$$

where $\Sigma(r_k) \in \mathbb{R}^{3 \times 3}$ is a positive definite symmetric matrix that is continuous in the position $r_k \in \mathbb{R}^2$. The square roots of the diagonal elements of $\Sigma(r_k)$ are the spatial and temporal decorrelation scales of the field. The decorrelation scales are the spatial and temporal separations at which the covariance function evaluates to $1/e \approx 0.368$. Note, for a stationary field, the decorrelation scales are constant, but for a nonstationary field they may vary in space and time. The covariance function (3) is used to derive the coordinate transformation in Section 4, which clusters measurements in space-time regions with short decorrelation scales, and spreads measurements elsewhere.

The statistics-based sensor-routing application of the DDDAS concept seeks to provide optimal coverage of an estimated spatiotemporal field. The coverage is deemed optimal when the measurement density in space and time is proportional to the variability of the field. To determine when measurements are redundant, we consider the footprint of a measurement, defined as the volume in space and time contained in an ellipsoid centered at the measurement location with principle axes equal to the decorrelation scales of the field. Figure 3 depicts two vehicles taking measurements along a circular trajectory in the space-time domain. The red and blue tubes along the vehicles' trajectories are the sensor swaths created by the measurement footprints. Figure 3(a) shows the swaths for a stationary field and Figure 3(b) shows the swaths for a nonstationary field in which the temporal scales contract at $t = 10$ hours. The goal is to design the vehicle trajectories so that the swaths created by the set of all measurement footprints cover the entire field with minimal overlaps or gaps, even when the decorrelation scales of the field vary.

To determine the mapping error, we employ optimal interpolation as in [6]. Consider the field $A(r)$ to be a discrete random field in space $r = (x, y)$ and time t . Let $\tilde{r}_d = [\tilde{x}_d, \tilde{y}_d, \tilde{t}_d]^T$ be the space-time location of measurement $d = 1, \dots, D$, where D is the total number of measurements taken by all of the vehicles, and ε_d be the measurement noise, so that the value of measurement d is $z_d = A(\tilde{r}_d) + \varepsilon_d$. We assume $E[\varepsilon_m \varepsilon_l] = \tilde{\sigma}_0 \delta_{ml}$, where $E[\cdot]$ denotes the expected value, $\tilde{\sigma}_0$ is the standard deviation of the measurement noise, and δ_{ml} is the Kronecker delta, which implies that the noise from any two distinct measurements is uncorrelated and the variance of the noise is $\tilde{\sigma}_0$.

Let C_e denote the covariance of the error in the estimate $\hat{A}(r)$ after assimilating the set of measurements $\tilde{r} = [\tilde{r}_1, \dots, \tilde{r}_D]^T$. We have

$$C_e(r_i, r_j; \tilde{r}) = C(r_i, r_j) - \sum_{d=1}^D \sum_{l=1}^D C(r_i, \tilde{r}_d)(M^{-1})_{dl} C(r_j, \tilde{r}_l),$$

as explained in [22, 9], where M^{-1} is the inverse of the measurement covariance matrix whose entries are [44]

$$M_{dl} = E[z_d z_l] = C(\tilde{r}_d, \tilde{r}_l) + \tilde{\sigma}_0 \delta_{dl}.$$

The mapping error is the diagonal of the error covariance matrix C_e . The average (resp. maximum) mapping error is computed by averaging (resp. finding the maximum of) all of the elements of the mapping error. Since the vehicles sample uniformly in time, the mapping error is minimized in a stationary field by traveling at maximum speed to place as many measurements as possible in the domain, as further illustrated in [58, 53]. Traveling as fast as possible may not be the best solution, however, for a nonstationary field, since one needs to slow down to concentrate more measurements in a space/time region of high variability.

3 Application I: Wake Estimation and Formation Control

3.1 Aerodynamic Model

This section illustrates the DDDAS concept using an observability-based sensor routing application originally presented in [43]. Consider two aircraft in steady level flight through an inviscid, incompressible, irrotational fluid. We employ an aerodynamic model of one aircraft flying in the other aircraft's wake, similar to that of Hemati et al. [30] and Pachter et al. [55]. Let the reference frame $\mathcal{B} = (O, \mathbf{b}_1, \mathbf{b}_2, \mathbf{b}_3)$ with origin O be attached to the center of the leading edge of the follower's wing with basis vectors. Assume that the follower aircraft maintains kinematic control of its vertical and horizontal velocities such that the velocity of frame \mathcal{B} with respect to the lead aircraft in steady level flight is $\mathbf{V}_f = V_y \mathbf{b}_2 + V_z \mathbf{b}_3$ (the \mathbf{b}_1 component is assumed to be zero). The leader has wingspan b and center position $\mathbf{r}_L = x_L \mathbf{b}_1 + y_L \mathbf{b}_2 + z_L \mathbf{b}_3$ relative to O . Assume $|x_L|$ is sufficiently large (i.e., greater than two wingspans [55]) such that the wake of the leader is adequately represented using potential flow theory as the sum of two infinite-line vortices, each with circulation strength Γ_L , extending horizontally behind the wingtips of the leader along the \mathbf{b}_1 direction. The Biot-Savart law gives the following vertical component of the wake [55, 30] w_L at a point (x, y, z) along the \mathbf{b}_2 axis ($x = z = 0$) as a function of the leader's position¹:

$$w_L(y; \Gamma_L, y_L, z_L, b) = \frac{\Gamma_L(y - y_L - b/2)}{2\pi(z_L^2 + (y - y_L - b/2)^2)} - \frac{\Gamma_L(y - y_L + b/2)}{2\pi(z_L^2 + (y - y_L + b/2)^2)}. \quad (4)$$

Note that (4) is symmetric about $z_L = 0$. This property necessitates invoking a second sensor to break the vertical symmetry. The aerodynamic signature on the follower aircraft created by the upwash field of the leader will be used to estimate the two-dimensional position $\mathbf{r} = (y_L, z_L)$ of the leader relative to the follower and the circulation strength Γ_L of the leader's wake. The position estimate $\hat{\mathbf{r}}$ will be used in an optimal controller to steer the follower to the desired relative position.

The flow around the follower aircraft in response to the upwash field of the leader is modeled by employing the lifting-line solution following Katz and Plotkin [36, p. 331–340]. For simplicity, assume the follower is represented by a flat, thin, rectangular wing with large aspect ratio ($\mathcal{R} > 4$) and chord length c . Since the fluid is inviscid, incompressible, and irrotational, its motion can be represented by the gradient of a potential function Φ that satisfies Laplace's equation [36]

$$\nabla^2 \Phi = 0. \quad (5)$$

In addition, at every point on the wing the potential function Φ must satisfy a boundary-value constraint that ensures that there is no flow normal to the wing surface. Assuming the wing is thin, its normal vector \mathbf{n}_i at any point (x_i, y_i, z_i) on the

¹ The notation $g(a, b; \alpha, \beta)$ represents a function $g(\cdot)$ that depends on the state variables a, b and the parameters α and β .

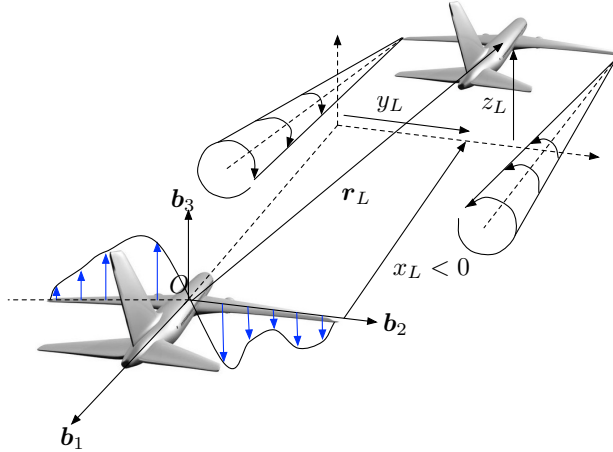


Fig. 4 Leader and follower aircraft representations. The wake of the leader produces an aerodynamic signature on the follower through its upwash field (blue). Reprinted from [43] with permission from the American Institute of Aeronautics and Astronautics.

wing surface is approximately $\mathbf{n}_i \approx \mathbf{b}_3$, $i = 1, \dots, N$, which implies

$$\nabla \Phi \cdot \mathbf{b}_3 = 0. \quad (6)$$

To satisfy these constraints, lifting-line theory constructs a suitable potential function from a collection of line vortices. N equally spaced horseshoe vortices are bound to the quarter chord of the follower aircraft wing such that $2N$ trailing vortices extending infinitely downstream. The i th bound horseshoe vortex has circulation strength Γ_i . The number N of horseshoe vortices must be chosen large enough for adequate model fidelity, yet small enough to remain computationally tractable. The freestream fluid velocity \mathbf{U}_∞ has magnitude U_∞ and angle of attack α relative to the wing. (Assume the freestream velocity has zero sideslip and α is small.)

Since the line vortex is a solution to Laplace's equation (5) [36], the flow due to the freestream velocity, leader aircraft upwash, and horseshoe vortices must satisfy the normal flow constraint (6). Therefore, (6) evaluated at any given point on the wing must satisfy

$$w_{hs} + w_L + V_z + U_\infty \sin \alpha = 0, \quad (7)$$

where w_{hs} is the \mathbf{b}_3 component of the flow generated by the horseshoe vortices, w_L is the vertical component of the leader aircraft's wake given by (4), V_z is the \mathbf{b}_3 component of the inertial velocity of the follower aircraft expressed in frame \mathcal{B} , and the fourth term on the left-hand side is the normal component of the freestream velocity. Note that this model neglects aerodynamic influences due to aircraft pitching, rolling, and sideslip maneuvers, under the assumption that in close proximity these motions are negligible relative to the aerodynamic effect of vertical motion.

To solve for the horseshoe vortex strengths Γ_i that satisfy (7), we employ the collocation method following Katz and Plotkin [36, p.331–334]. Impose the constraint (7) at N collocation points centered at each horseshoe vortex along the 3/4-chord line. Since the flow at any collocation point is linearly dependent on the circulation strength Γ_i of the i th horseshoe vortex, (7) applied at the N collocation points forms a set of N linear algebraic equations with N unknown circulation strengths [36] Γ_i , $i = 1 \dots, N$,

$$\begin{bmatrix} a_{11} & \cdots & a_{1N} \\ \vdots & \ddots & \vdots \\ a_{N1} & \cdots & a_{NN} \end{bmatrix} \begin{bmatrix} \Gamma_1 \\ \vdots \\ \Gamma_N \end{bmatrix} = -(U_\infty \sin \alpha + V_z) \begin{bmatrix} 1 \\ \vdots \\ 1 \end{bmatrix} - \begin{bmatrix} w_L(y_1) \\ \vdots \\ w_L(y_N) \end{bmatrix}. \quad (8)$$

Here

$$\sum_{i=1}^N a_{ji} \Gamma_i = w_{hs}(y_j), \quad (9)$$

is the normal component of the flow at the j collocation point, V_z is the (control) velocity of the follower aircraft, and $w_L(y_j)$ is obtained by evaluating (4) at y_j . Equation (8) is solved for the circulation strength distribution $\Gamma_1, \dots, \Gamma_N$ by inverting the a_{ji} coefficient matrix [36].

The circulation strength distribution $\Gamma(y) = \lim_{N \rightarrow \infty} \Gamma_i$ is used to calculate measurable quantities that will be used in the nonlinear wake estimation process. For example, Hemati et al. [30] use the following measurements of the differential pressure coefficient ΔC_p :

$$\Delta C_p(x, y) = \frac{-4\Gamma(y)}{\pi U_\infty c} \left(\frac{c}{x} - 1 \right)^{1/2}. \quad (10)$$

Assume the measurements of differential pressure are equally spaced on the 3/4-chord line $x = (3c)/4$ along the span of the wing.

Let $\mathbf{h}(\boldsymbol{\Omega}) = [\Delta C_{p1} \dots \Delta C_{pP}]^T$ be a $P \times 1$ column matrix of differential pressure measurements calculated using (10) on the 3/4-chord line, where P is the number of measurements. Taking $\mathbf{h}(\boldsymbol{\Omega})$ as the output and using the leader aircraft dynamics in frame \mathcal{B} , generates the following state-space form of the input-output relationship between the wake parameter states $\boldsymbol{\Omega} = [y_L, z_L, \Gamma_L]^T$ and the measurements $\boldsymbol{\phi}$:

$$\begin{aligned} \dot{\boldsymbol{\Omega}} &= \begin{bmatrix} -V_y \\ -V_z \\ 0 \end{bmatrix} \\ \boldsymbol{\phi} &= \mathbf{h}(\boldsymbol{\Omega}). \end{aligned} \quad (11)$$

The model (11) is used to evaluate the observability of the state $\boldsymbol{\Omega}$ with the output equation $\mathbf{h}(\boldsymbol{\Omega})$, design an observer to estimate $\boldsymbol{\Omega}$ from noisy output measurements, and implement an optimal control strategy for the follower aircraft.

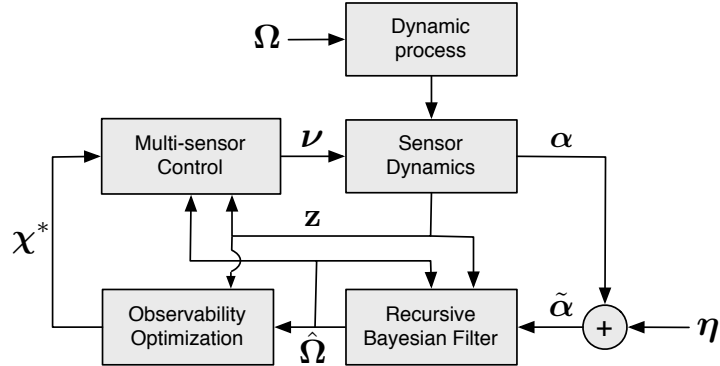


Fig. 5 A schematic diagram of an observability-based sampling algorithm. A recursive Bayesian filter provides parameter estimates $\hat{\Omega}$ from noisy measurements $\tilde{\alpha}$. The estimated parameters are used to calculate observability optimizing control parameters χ^* that characterize the multi-sensor sampling formation.

3.2 Formation Flight Control

The optimal control approach described here incorporates a weighted wavefront expansion, known as the fast marching method [61], to generate an optimal cost-to-go potential map relative to the desired position of the lead aircraft. The gradient of this potential function provides the optimal control with respect to an observability-based cost function. This method does not require iterative calculation of the control since the potential is calculated over the entire relative position space, making the control computationally less expensive than a receding-horizon control [43].

The optimal path planning problem is formulated as follows [61, pg. 284–291]. Given a desired position \mathbf{r}_{des} , the goal is to find the path $\mathcal{L}(l) : [0, \infty) \rightarrow \mathbb{R}^2$ from \mathbf{r}_{des} to any point \mathbf{r}_0 that minimizes the observability-based cost integral [61]

$$\int_{\mathbf{r}_{des}}^{\mathbf{r}_0} \log \xi(\mathcal{L}(l)) dl,$$

where l is the arc-length parameterization of the path \mathcal{L} and $\xi(\cdot)$ is the unobservability index evaluated along \mathcal{L} . Let the minimum cost required to travel from \mathbf{r}_{des} to a point \mathbf{r} be [61]

$$J_{WF}(\mathbf{r}) \triangleq \min_{\mathcal{L}} \int_{\mathbf{r}_{des}}^{\mathbf{r}} \xi(\mathcal{L}(l)) dl, \quad (12)$$

such that the level set $J_{WF}(\mathbf{r}) = C$ is the set of points that can be reached with minimal cost C . By construction, level sets are orthogonal to the minimal cost paths [61] implying that the optimal path descends the gradient of $J_{WF}(\mathbf{r})$.

The fast marching method [61] is a wavefront propagation technique that is used to efficiently compute $J_{WF}(\mathbf{r})$ for the domain around the leader aircraft [61, pg. 86–99]. Since the optimal path descends the gradient of $J_{WF}(\mathbf{r})$, an observer-based feed-

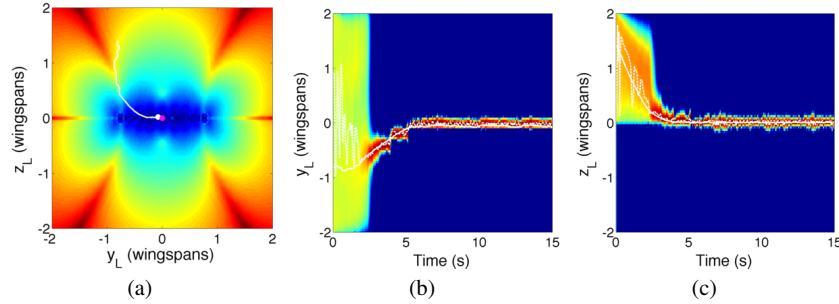


Fig. 6 Simulation illustrating aerial refuel positioning with optimal control algorithm using wavefront-propagation method. (a) Trajectory; (b) marginal probability densities of Bayesian filter. Reprinted from [43] with permission from the American Institute of Aeronautics and Astronautics.

back control incorporates estimates of the relative position $\hat{\mathbf{r}}$ according to

$$\mathbf{u} = -K_{WF} \nabla J_{WF}(\hat{\mathbf{r}}), \quad (13)$$

where the gain $K_{WF} > 0$. Assuming the desired final location is fixed, the cost potential $J_{WF}(\mathbf{r})$ need be calculated only once to produce all possible optimal paths.

Numerical simulations of the wavefront-propagation control strategy were computed for the follower aircraft positioning itself for aerial refueling. The simulation assumes noise $\Sigma = 10^{-5}$ in the differential pressure coefficient measurements and total simulation time $T = 15$ seconds. A recursive Bayesian filter assimilates measurements at 5 Hz [43]. The wavefront-propagation control strategy has gain $K_{WF} = 5$ for all simulations. In aerial refueling the follower aircraft intercepts a filling nozzle that extends outward from the tail of the leader [18] by maintaining a desired relative position of $\mathbf{r}_{des} = (0, 0)$ wingspans. This implementation assumes the aerodynamic effects of the filling nozzle on the follower aircraft are minimal at the sensor positions. Figure 6 depicts the simulations results, which show the trajectory converging to the desired position along a path of guaranteed observability of the leader aircraft's relative position.

4 Application II: Coverage Control of a Nonstationary Field

4.1 Coordinate Transformation

This section defines a nonlinear coordinate transformation that renders a nonstationary field locally stationary, following [54]. The significance of this transformation is that it permits the use of multi-vehicle sampling algorithms designed for use in stationary fields. We derive two transformations, one for which the spatial decorre-

lation scales are coupled, i.e., $\sigma_x = \sigma_x(x_k, y_k)$ and $\sigma_y = \sigma_y(x_k, y_k)$, and another for which the spatial scales are decoupled, i.e., $\sigma_x = \sigma_x(x_k)$ and $\sigma_y = \sigma_y(y_k)$.

Let $r_k \triangleq [x_k, y_k, t_k]^T$ be the space-time coordinates in the original domain, called the r -domain, and $R_k \triangleq [X_k, Y_k, T_k]^T$ be a set of transformed coordinates in a new domain, called the R -domain. Also, let $G(V, E)$ be a lattice graph with nodes V placed at each R_k and undirected edges E connecting adjacent cells (the four nearest neighbors in two dimensions). The lattice graph ensures that adjacent nodes are locally stationary under the transformation. We would like to find R_k such that the field with covariance (3) becomes locally stationary, i.e., all adjacent nodes in G are (approximately) stationary, as in [60]. Intuitively, this corresponds to ensuring that the field is stationary in the neighborhood of each point R_k . Let $\bar{\Sigma}(r_i, r_j) = (\Sigma(r_i) + \Sigma(r_j))/2$, $r_{ij} \triangleq r_i - r_j$, and $R_{ij} \triangleq R_i - R_j$. Thus, we seek to satisfy

$$\frac{|\Sigma(r_i)|^{1/4} |\Sigma(r_j)|^{1/4}}{\sqrt{|\bar{\Sigma}(r_i, r_j)|}} e^{-[r_{ij}^T(\bar{\Sigma}(r_i, r_j))^{-1} r_{ij}]} = e^{-[R_{ij}^T R_{ij}]} \quad (14)$$

between all adjacent points i and j . The left-hand side of (14) is the nonstationary covariance function in the r -domain and the right hand side is the covariance function in the R -domain, which we desire to be stationary. Without loss of generality, the spatial and temporal decorrelation scales in the R -domain are chosen to be $\sigma_X = \sigma_Y = \tau_T = 1$. Since the spatial decorrelation scales are coupled, the transformations are also coupled; however, the temporal component of (14) is decoupled by assumption. Let $\sigma_{xi} \triangleq \sigma_x(x_i, y_i)$, $\sigma_{yi} \triangleq \sigma_y(x_i, y_i)$, and $\tau_i \triangleq \tau(t_i)$. Then, (14) yields the following two relations:

$$(X_i - X_j)^2 + (Y_i - Y_j)^2 = \frac{2(x_i - x_j)^2}{\sigma_{xi}^2 + \sigma_{xj}^2} + \frac{2(y_i - y_j)^2}{\sigma_{yi}^2 + \sigma_{yj}^2} + \ln \left[\left(\frac{\sigma_{xi}^2 + \sigma_{xj}^2}{2\sigma_{xi}\sigma_{xj}} \right) \left(\frac{\sigma_{yi}^2 + \sigma_{yj}^2}{2\sigma_{yi}\sigma_{yj}} \right) \right] \quad \text{and} \quad (15)$$

$$(T_i - T_j)^2 = \frac{2(t_i - t_j)^2}{\tau_i^2 + \tau_j^2} + \ln \left(\frac{\tau_i^2 + \tau_j^2}{2\tau_i\tau_j} \right). \quad (16)$$

Equations (15) and (16) show how the space-time separation between two points in the R -domain depends on the nonstationarity in the r -domain. However, to complete the spatial transformation we need another relationship between $X_{ij} \triangleq X_i - X_j$ and $Y_{ij} \triangleq Y_i - Y_j$ to separate (15) into two equations. We use the orientation between points in the R -domain and r -domain. The relation

$$\tan \left(\frac{Y_i - Y_j}{X_i - X_j} \right) = \tan \left(\frac{y_i - y_j}{x_i - x_j} \right) \quad (17)$$

preserves the relative orientation between points i and j , which ensures that the transformation will not rotate the coordinates in the R -domain, as it does in [60].

Substituting (17) in (15) we obtain

$$X_{ij} = \pm \left[\frac{2(x_i - x_j)^2}{\sigma_{xi}^2 + \sigma_{xj}^2} + \frac{2(y_i - y_j)^2}{\sigma_{yi}^2 + \sigma_{yj}^2} + \ln \left[\left(\frac{\sigma_{xi}^2 + \sigma_{xj}^2}{2\sigma_{xi}\sigma_{xj}} \right) \left(\frac{\sigma_{yi}^2 + \sigma_{yj}^2}{2\sigma_{yi}\sigma_{yj}} \right) \right]^{1/2} \times \left(1 + \frac{y_i - y_j}{x_i - x_j} \right)^{-1} \right] \triangleq d_{X,ij}, \quad (18)$$

$$Y_{ij} = \pm \left[\frac{2(x_i - x_j)^2}{\sigma_i^2 + \sigma_j^2} + \frac{2(y_i - y_j)^2}{\sigma_i^2 + \sigma_j^2} + \ln \left[\left(\frac{\sigma_{xi}^2 + \sigma_{xj}^2}{2\sigma_{xi}\sigma_{xj}} \right) \left(\frac{\sigma_{yi}^2 + \sigma_{yj}^2}{2\sigma_{yi}\sigma_{yj}} \right) \right]^{1/2} \times \left(1 + \frac{x_i - x_j}{y_i - y_j} \right)^{-1} \right] \triangleq d_{Y,ij}, \quad \text{and} \quad (19)$$

$$T_i - T_j = \pm \left[\frac{2(t_i - t_j)^2}{\tau_i^2 + \tau_j^2} + \ln \left(\frac{\tau_i^2 + \tau_j^2}{2\tau_i\tau_j} \right) \right]^{1/2} \triangleq d_{T,ij}. \quad (20)$$

Equations (18)–(20) represent the transformation from the r -domain to the R -domain. Note that the choice of plus or minus in (18)–(20) is arbitrary as it represents flipping the new coordinates about the corresponding axis. Thus, we use the positive root.

Let B be the incidence matrix of the lattice graph G . We rewrite (18)–(20) as

$$B^T X = d_X, \quad B^T Y = d_Y, \quad \text{and} \quad B^T T = d_T, \quad (21)$$

where d_X is the vector of all terms $d_{X,ij}$ and d_Y and d_T are defined similarly. These equations are, in general, overdetermined. The least-squares solution to (21) is obtained using the pseudoinverse. The use of the lattice graph topology is justified since points with short separation (in space or time) have a stronger impact on the mapping error than points with large separation. We have also found the lattice topology to be particularly sensitive to nonstationarities in the r -domain; higher connected graphs tend to concentrate measurements less.

The inverse transformation from the R -domain to the r -domain is solved by creating a lookup table as follows. A uniform grid is created in the r -domain and mapped to the R -domain, which produces a nonuniform grid of locations in the R -domain. Trajectories generated in the R -domain are discretized and mapped back to the r -domain by interpolating this grid. Figure 7 shows an example of the two-dimensional spatial transformation using decorrelation scales σ_x and σ_y and a varying spatial decorrelation scale where a “dip” in the scales is centered at (3, 3). On the right is the r -domain, which has a square boundary. When the r -domain boundary is mapped to the R -domain, it generates a new, curved boundary. A uniform grid mapped from the R -domain to the r -domain shows how space is warped to concentrate measurements near the nonstationarity. For the conditions that guarantee the mapping is invertible, the reader is referred to [54].

Next, consider when the spatial decorrelation scales are decoupled, i.e., $\sigma_{xi} = \sigma_x(x_i)$ and $\sigma_{yi} = \sigma_y(y_i)$. In this case, (18)–(20) reduce to

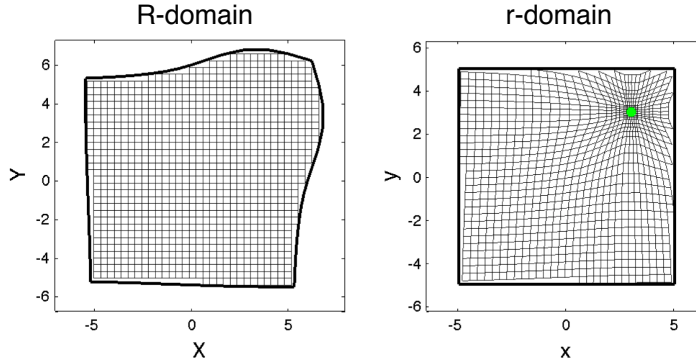


Fig. 7 Example of the spatial transformation with a nonstationarity at (3,3). Reprinted from [54] with permission from Elsevier.

$$X_i - X_j = \left[\frac{2(x_i - x_j)^2}{\sigma_{xi}^2 + \sigma_{xj}^2} + \ln \left(\frac{\sigma_{xi}^2 + \sigma_{xj}^2}{2\sigma_{xi}\sigma_{xj}} \right) \right]^{1/2}, \quad (22)$$

$$Y_i - Y_j = \left[\frac{2(y_i - y_j)^2}{\sigma_{yi}^2 + \sigma_{yj}^2} + \ln \left(\frac{\sigma_{yi}^2 + \sigma_{yj}^2}{2\sigma_{yi}\sigma_{yj}} \right) \right]^{1/2}, \text{ and} \quad (23)$$

$$T_i - T_j = \left[\frac{2(t_i - t_j)^2}{\tau_i^2 + \tau_j^2} + \ln \left(\frac{\tau_i^2 + \tau_j^2}{2\tau_i\tau_j} \right) \right]^{1/2}. \quad (24)$$

For a lattice topology with decoupled decorrelation scales, we have $j = i + 1$, i.e., $X_j = X_i + \Delta X_i$, $x_j = x_i + \Delta x_i$ (and similarly for Y , y , T , and t). Taking the limit as the lattice spacing goes to zero yields the following analytical approximation of (22)–(24):

$$X_k = \int_0^{x_k} \frac{1}{\sigma_x(x')} dx', \quad (25)$$

$$Y_k = \int_0^{y_k} \frac{1}{\sigma_y(y')} dy', \quad \text{and} \quad (26)$$

$$T_k = \int_0^{t_k} \frac{1}{\tau(t')} dt'. \quad (27)$$

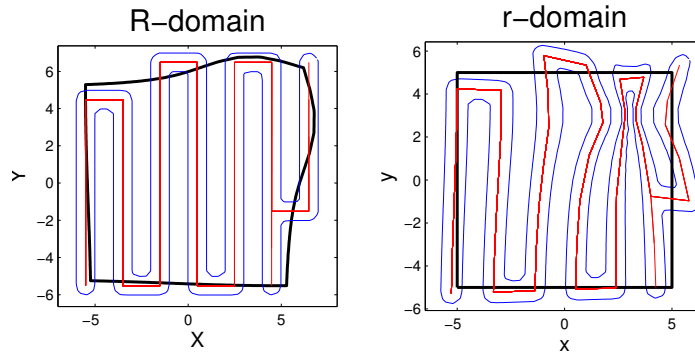


Fig. 8 Example of the spatial transformation of an operating domain (black) and a sampling trajectory (blue) generated from a spanning-tree coverage algorithm (red). Reprinted from [54] with permission from Elsevier.

The transformation (25)–(27) exists and is invertible if $\sigma(x_k)$, $\sigma(y_k)$, and $\tau(t_k)$ are positive, bounded, and continuous functions. Either the numerical or analytical form of the transformation presented above can be used for sampling a nonstationary spatiotemporal field, but the numerical transformation has the advantage that it is valid for any function of the decorrelation scales (as long as they are continuous and positive); however, it has (relatively) stringent conditions for invertibility [54]. The analytical transformation is always invertible when the decorrelation scales are positive, but it is only valid when the spatial scales are decoupled.

4.2 Multi-vehicle Coverage Control

This section describes a multi-vehicle coverage algorithm that invokes the coordinate transformation from the previous section to generate nonuniform sampling trajectories [54]. We first implement a multi-vehicle controller that uniformly covers the R -domain. To ensure that the R -domain is uniformly covered with no gaps or overlaps between sensor measurements, we employ without loss of generality an existing coverage algorithm called Spanning Tree Coverage (STC) [21]. Intuitively, the algorithm works like a lawn-mowing algorithm along a closed path. Path closure is crucial due to the temporal nature of the field; locations are revisited to ensure that the temporal variation of the field is captured. As an example, consider the spatial scale function with a solitary contraction of the decorrelation scales and the sampling boundary in Figure 7. Figure 8 shows the spanning tree and generated path in the R -domain (left) and the r -domain (right).

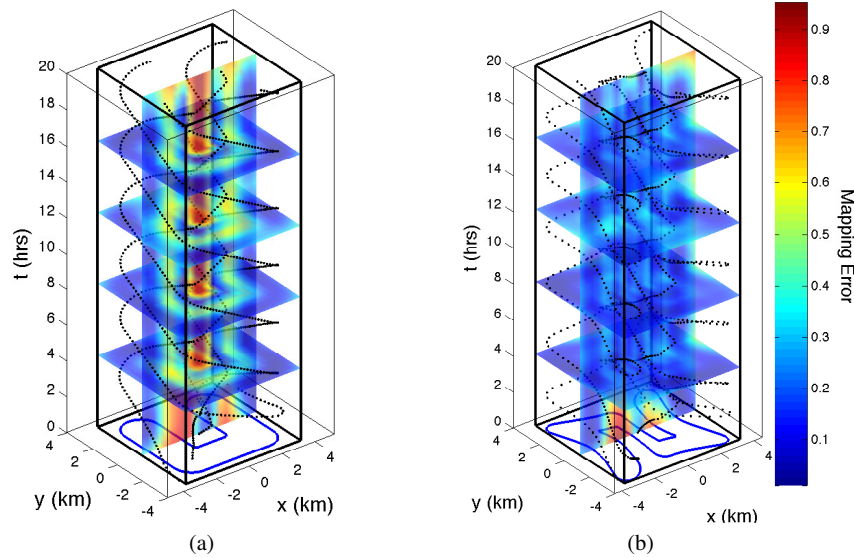


Fig. 9 Mapping error of a 3D nonstationary spatiotemporal field using (a) uniform sampling and (b) a nonstationary sampling algorithm. Reprinted from [54] with permission from Elsevier.

We seek to steer a set of mobile vehicles to motion along the path generated by the STC algorithm. The vehicles maintain equal spacing from one another along the path. To illustrate the algorithm, we performed a simulation of twelve vehicles with random initial conditions. The trajectories in the R -domain are transformed back to the r -domain by numerically inverting the coordinate transformation. In the r -domain, vehicles cluster their measurements in the area of the dip to ensure that the full domain is covered, even in areas where the spatial and temporal decorrelation scales are small. Figure 9 shows the resulting mapping error in comparison to a uniform sampling algorithm. There is a dip in the decorrelation scales centered at $x_{0,1} = y_{0,1} = 0$ km, and $t = 12$ hours. Five vehicles travel along a closed path in the r -domain. The blue curve on the $t = 0$ plane shows the spatial path that the vehicles track. The average mapping error is 0.271 using uniform coverage (Figure 7(a)) and 0.178 when using the nonstationary sampling algorithm (Figure 7(b)). Likewise, the maximum error is reduced from 0.983 to 0.768.

5 Summary

This report describes a DDDAS project that optimizes vehicle routing using two different strategies. The first strategy is based on maximizing observability of an unknown process, e.g., a flow field. This strategy is applied to an aircraft refuel-

ing scenario in which the trailing aircraft uses distributed pressure sensors to center its position on the wake of the lead aircraft. The observability of the leader aircraft is assessed using measures of the empirical observability gramian and a recursive Bayesian filter is implemented to estimate the leader's wake parameters. A wavefront-propagation optimal control algorithms invokes the unobservability index as a cost metric and incorporate estimates of the leader's state provided by a Bayesian filter. Numerical simulations of formation flight and aerial refueling applications illustrate that the control algorithm successfully steers the vehicle to a desired relative position using the estimated the wake parameters.

The second strategy for DDDAS vehicle routing is based on a statistical representation of an unknown spatiotemporal process. This strategy is applied to achieve non-uniform coverage of a spatiotemporal environmental field. We describe a multi-vehicle control algorithm that generate nonuniform coverage of a nonstationary spatiotemporal field by using a coordinate transformation to render the field locally stationary in a new set of coordinates (the R -domain). Existing spatial coverage and path sampling algorithms produce trajectories that uniformly sample the R -domain; in the original coordinates (the r -domain), these trajectories concentrate measurements near regions of high variability.

The DDDAS concept manifests itself in both applications described in this report in the following sense: measurement data from a distributed sensor array is assimilated into a model of an estimated process, which is in turn used to guide the collection of subsequent measurements. The report describes new capabilities with regards to observability-based sensor path-planning and adaptive sampling of non-stationary processes for which non-uniform coverage is required. Ongoing directions of research include solving the co-array problem: i.e., simultaneous mapping and estimation decorrelation scales, also known as hyperparameters.

References

1. N. U. Ahmed and C. D. Charalambous. Optimal measurement strategy for nonlinear filtering. *SIAM J. Control Optim.*, 45(2):519–531, 2006.
2. A. Alvarez and B. Mourre. Optimum sampling designs for a glider–mooring observing network. *J. Atmospheric and Oceanic Technology*, 29(4):601–612, 2011.
3. A. Alvarez and E. Reyes. Volumetric estimation of thermal fields inferred from glider-like and remote-sensing measurements in undersampled coastal regions. *J. Geophysical Research*, 115(C11006):13, 2010.
4. D. Baronov and J. Baillieul. Decision making for rapid information acquisition in the reconnaissance of random fields. *Proc. IEEE*, 100(3):776–801, 2012.
5. N. Barth and C. Wunsch. Oceanographic experiment design by simulated annealing. *J. Physical Oceanography*, 20(9):1249–1263, 1990.
6. A. F. Bennett. *Inverse Modeling of the Ocean and Atmosphere*. Cambridge University Press, 2005.
7. C. H. Bishop, B. J. Etherton, and S. J. Majumdar. Adaptive sampling with the ensemble transform Kalman filter. Part I: Theoretical aspects. *Monthly Weather Review*, 129(3):420–436, 2001.
8. M. K. Biswas and T. N. Krishnamurti. Adaptive use of research aircraft data sets for hurricane forecasts. *Meteorol. Atmos. Phys.*, 99(1-2):1–2, 2008.

9. F. P. Bretherton, R. E. Davis, and C. B. Fandry. A technique for objective analysis and design of oceanographic experiments applied to MODE-73. *Deep-Sea Research*, 23(7):559–582, 1976.
10. T. Campbell, S. Ponda, G. Chowdhary, and J. P. How. Planning under uncertainty using non-parametric Bayesian models. In *Proc. AIAA Conf. Guidance, Navigation, and Control*, number AIAA 2012-4682, Minneapolis, Minnesota, August 2012.
11. M. Chapouly and M. Mirrahimi. Distributed source identification for wave equations: An offline observer-based approach. *IEEE Trans. Automatic Control*, 57(8):2067–2073, 2012.
12. H.-L. Choi and J. P. How. Coordinated targeting of mobile sensor networks for ensemble forecast improvement. *IEEE Sensors J.*, 11(3):621–633, 2011.
13. H.-L. Choi and J. P. How. Efficient targeting of sensor networks for large-scale systems. *IEEE Trans. Control Systems Technology*, 19(6):1569–1577, 2011.
14. J. Choi, S. Oh, and R. Horowitz. Distributed learning and cooperative control for multi-agent systems. *Automatica*, 25(12):2802–2814, 2009.
15. J. Das, F. Py, T. Maughan, T. O'Reilly, M. Messié, J. Ryan, G. S. Sukhatme, and K. Rajan. Coordinated sampling of dynamic oceanographic features with underwater vehicles and drifters. *Int. J. Robotics Research*, 31(5):626–646, 2012.
16. R. E. Davis, N. E. Leonard, and D. M. Fratantoni. Routing strategies for underwater gliders. *Deep-Sea Research II*, 56(3–5):173–187, 2009.
17. M. A. Demetriou. Guidance of mobile actuator-plus-sensor networks for improved control and estimation of distributed parameter systems. *IEEE Trans. Automatic Control*, 55(7):1570–1584, 2010.
18. A. Dogan, S. Sato, and W. Blake. Flight control and simulation for aerial refueling. In *In Proc. of AIAA Guidance, Navigation, and Control Conf.*, San Francisco, CA, August 2005.
19. M. Dunbabin and L. Marques. Robotics for environmental monitoring. *IEEE Robotics & Automation Magazine*, 19(1):24–39, 2012.
20. H. J. S. Feder, J. J. Leonard, and C. M. Smith. Adaptive mobile robot navigation and mapping. *Int. J. Robotics Research*, 18(7):650–668, 1999.
21. Y. Gabriely and E. Rimon. Spanning-tree based coverage of continuous areas by a mobile robot. *Annals of Mathematics and Artificial Intelligence*, 31, 2001.
22. L. S. Gandin. *Objective Analysis of Meteorological Fields*. Israel Program for Scientific Translations, Jerusalem, 1965.
23. A. García-Olaya, F. Py, J. Das, and K. Rajan. An online utility-based approach for sampling dynamic ocean fields. *IEEE J. Oceanic Engineering*, 37(2):185–203, 2012.
24. R. Graham and J. Cortés. Adaptive information collection by robotic sensor networks for spatial estimation. *IEEE Trans. Automatic Control*, 57(6):1404–1419, 2012.
25. F. Grasso. Case study 1: How robotic lobsters locate odour sources in turbulent water. In O. Holland and D. McFarland, editors, *Artificial Ethology*, chapter 3, pages 47–59. Oxford University Press, 2001.
26. B. Grocholsky. *Information-Theoretic Control of Multiple Sensor Platforms*. PhD thesis, University of Sydney, 2002.
27. D. Grünbaum. Schooling as a strategy for taxis in a noisy environment. In J. K. Parrish and W. M. Hamner, editors, *Animal Groups in Three Dimensions*, chapter 17, pages 257–281. Cambridge University Press, 1987.
28. J. Hahn and T. F. Edgar. A gramian based approach to nonlinear quantification and model classification. *Industrial and Engineering Chemistry Research*, 40:5724–5731, 2001.
29. K. D. Heaney, G. Gawarkiewicz, T. F. Duda, and P. F. J. Lermusiaux. Nonlinear optimization of autonomous undersea vehicle sampling strategies for oceanographic data-assimilation. *J. Field Robotics*, 24(6):437–448, 2007.
30. M. S. Hemati, J. D. Eldredge, and J. L. Speyer. Wake sensing for aircraft formation flight. In *Proc. AIAA Guidance, Navigation and Control Conf.*, number AIAA 2012-4768, page 8pp, Minneapolis, Minnesota, August 2012.
31. R. Hermann and A. J. Krener. Nonlinear controllability and observability. *IEEE Trans. Automatic Control*, AC-22(5):728–740, 1977.

32. J. Hespanha. *Linear Systems Theory*. Princeton University Press, 2009.
33. D. Higdon, J. Swall, and J. Kern. Non-stationary spatial modeling. In *Bayes. Stat.* 6, pages 761–768. Oxford UP, 1999.
34. G. M. Hoffmann and C. J. Tomlin. Mobile sensor network control using mutual information methods and particle filters. *IEEE Trans. Automatic Control*, 55(1):32–47, 2010.
35. Karspeck, Kaplan, and Sain. Bayesian modelling and ensemble reconstruction of mid-scale spatial variability in North Atlantic sea-surface temperatures for 1850-2008. *Q. J. R. Meteorol. Soc.*, 138(662):234–248, 2012.
36. J. Katz and A. Plotkin. *Low-Speed Aerodynamics*. Cambridge University Press, second edition, 2001.
37. A. Krener. Eulerian and lagrangian observability of point vortex flows. *Tellus A*, 60(5):1089–1102, 2008.
38. A. J. Krener and K. Ide. Measures of unobservability. In *Proc. IEEE Conf. Decision and Control*, pages 6401–6406, Shanghai, China, December 2009.
39. M. Kumar, K. Cohen, and B. HomChaudhuri. Cooperative control of multiple uninhabited aerial vehicles for monitoring and fighting wildfires. *J. Aerospace Computing, Information, and Communication*, 8(1):1–16, 2011.
40. S. Lall, J. E. Marsden, and S. Glavaški. Empirical model reduction of controlled nonlinear systems. In *Proc. IFAC World Congress*, pages 473–478, Beijing, China, July 1999.
41. S. Lall, J.E. Marsden, and S.A. Glavaski. A subspace approach to balanced truncation for model reduction of nonlinear control systems. *Int. J. of Robust and Nonlinear Cont.*, 12(6):519–535, 2002.
42. L. DeVries, S. J. Majumdar, and D. A. Paley. Observability-based optimization of coordinated sampling trajectories for recursive estimation of a strong, spatially varying flowfield. *J. Intelligent and Robotic Systems*, 67(3-4):527–544, 2012.
43. L. DeVries and D. A. Paley. Wake estimation and dynamic control for autonomous aircraft in formation flight. In *Proc. AIAA Conf. Guidance, Navigation, and Control*, number AIAA-2013-4705, Boston, Massachusetts, August 2013.
44. N. E. Leonard, D. A. Paley, F. Lekien, R. Sepulchre, D. M. Fratantoni, and R. E. Davis. . *Proc. IEEE*, 95(1):48–74, 2007.
45. P. F. J. Lermusiaux. Adaptive modeling, adaptive data assimilation and adaptive sampling. *Physica D*, 230(1-2):172–196, 2007.
46. P. B. Liebelt. *An Introduction to Optimal Estimation*. Addison-Wesley, 1967.
47. D. Maessen and E. Gill. Relative state estimation and observability analysis for formation flying satellites. *J. Guidance, Control, and Dynamics*, 35(1):321–326, 2012.
48. S. J. Majumdar, C. H. Bishop, and B. J. Etherton. Adaptive sampling with the ensemble transform Kalman filter. Part II: Field program implementation. *Monthly Weather Review*, 130(5):1356–1369, 2002.
49. A. Manufo, E. Simetti, A. Turetta, A. Caiti, and G. Casalino. Autonomous underwater vehicle teams for adaptive ocean sampling: a data-driven approach. *Ocean Dynamics*, pages 1–14, 2011. 10.1007/s10236-011-0464-x.
50. T. W. Mather and M. A. Hsieh. Macroscopic modeling of stochastic deployment policies with time delays for robot ensembles. *Int. J. Robotics Research*, 30(5):590–600, 2011.
51. G. Mathew and I. Mezić. Metrics for ergodicity and design of ergodic dynamics for multi-agent systems. *Physica D*, 240:432–442, 2011. doi:10.1016/j.physd.2010.10.010.
52. W. G. Müller. *Collecting Spatial Data*. Physica-Verlag, 2nd edition, 2001.
53. N. Sydney and D. A. Paley. Multi-vehicle control and optimization for spatiotemporal sampling. In *Proc. IEEE Conf. Decision and Control*, pages 5607–5612, Orlando, Florida, December 2011. Invited session on “Consensus algorithms, cooperative control, and distributed optimization”.
54. N. Sydney and D. A. Paley. Multivehicle coverage control for nonstationary spatiotemporal fields. *Automatica*, 50(5):1381–1390, 2014.
55. M. Pachter, J. J. D’Azzo, and A. W. Proud. Tight formation flight control. *AIAA J. of Guidance, Control, and Dynamics*, 24(2):246–254, March-April 2001.

56. C. J. Paciorek. *Nonstationary Gaussian Processes for Regression and Spatial Modelling*. PhD thesis, Carnegie Mellon University, Pittsburgh, Pennsylvania, 2003.
57. C. J. Paciorek and M. J. Schervish. Spatial modelling using a new class of nonstationary covariance functions. *Environmetrics*, 17(5):483–506, 2006.
58. D. A. Paley. *Cooperative control of collective motion for ocean sampling with autonomous vehicles*. PhD thesis, Princeton University, Princeton, New Jersey, September 2007.
59. C. A. Reynolds, M. S. Peng, S. J. Majumdar, S. D. Aberson, C. H. Bishop, and R. Buizza. Interpretation of adaptive observing guidance for Atlantic tropical cyclones. *Monthly Weather Review*, 135(12):4006–4029, 2007.
60. P. D. Sampson and P. Guttorp. Nonparametric estimation of nonstationary spatial covariance structure. *J. American Statistical Association*, 87(417):108–119, 1992.
61. J. A. Sethian. *Level set methods and fast marching methods: evolving interfaces in computational geometry, fluid mechanics, computer vision, and materials science*. Cambridge University Press, 1999.
62. A. Singh, A. Krause, and W. Kaiser. Nonmyopic adaptive informative path planning for multiple robots. In *Proc. Int. Joint Conf. Artificial Intelligence*, pages 1843–1850, Pasadena, California, July 2009.
63. A. Singh, R. Nowak, and P. Ramanathan. Active learning for adaptive mobile sensing networks. In *Proc. 5th Int. Conf. Information Processing in Sensor Networks*, Nashville, Tennessee, April 2006. doi: 10.1145/1127777.1127790.
64. S. Skogestad and I. Postlethwaite. *Multivariable Feedback Control: Analysis and Design*. Wiley and Sons, West Sussex, England, 1996.
65. R. N. Smith, Y. Chao, B. H. Jones, D. A. Caron, P. P. Li, and G. S. Sukhatme. Trajectory design for autonomous underwater vehicles based on ocean model predictions for feature tracking. *Field and Service Robotics*, 62:263–273, 2010.
66. R. N. Smith, Y. Chao, P. P. Li, D. A. Caron, B. H. Jones, and G. S. Sukhatme. Planning and implementing trajectories for autonomous underwater vehicles to track evolving ocean processes based on predictions from a regional ocean model. *Int. J. Robotics Research*, 29(12):1475–1497, 2010.
67. S. L. Smith, M. Schwager, and D. Rus. Persistent tasks for robots in changing environments. Submitted to *IEEE Trans. Robotics*, 2010.
68. S. Sokolov and S. R. Rintoul. Some remarks on interpolation of nonstationary oceanographic fields. *J. Atmos. Oceanic Tech.*, 16(10):1434–1449, 1999.
69. C. Song, G. Feng, Y. Fan, and Y. Wang. Decentralized adaptive awareness coverage control for multi-agent networks. *Automatica*, 47(12):2749–2756, 2011.
70. S. K. Thompson. *Sampling*. John Wiley & Sons, 2nd edition, 2002.
71. Y. Xiong, W. Chen, D. Apley, and X. Ding. A non-stationary covariance-based Kriging method for metamodelling in engineering design. *Int. J. Numerical Methods in Engineering*, 71(6):733–756, 2007.
72. Y. Xu, J. Choi, and S. Oh. Mobile sensor network navigation using Gaussian processes with truncated observations. *IEEE Trans. Robotics*, 27(6):1118–1131, 2011.
73. N. K. Yilmaz, C. Evangelinos, P. F. J. Lermusiaux, and N. M. Patrikalakis. Path planning of autonomous underwater vehicles for adaptive sampling using mixed integer linear programming. *IEEE J. Oceanic Engineering*, 33(4):522–537, 2008.
74. H. Yu, R. Sharma, R. W. Beard, and C. N. Taylor. Observability-based local path planning and collision avoidance for micro air vehicles using bearing-only measurements. In *Proc. American Control Conf.*, pages 4649–4654, San Francisco, California, June 2011.
75. F. Zhang and N. E. Leonard. Cooperative filters and control for cooperative exploration. *IEEE Trans. Automatic Control*, 55(3):650–663, 2010.

AFOSR Deliverables Submission Survey

Response ID:6939 Data

1.

Report Type

Final Report

Primary Contact Email

Contact email if there is a problem with the report.

dpaley@umd.edu

Primary Contact Phone Number

Contact phone number if there is a problem with the report

3014055757

Organization / Institution name

University of Maryland

Grant/Contract Title

The full title of the funded effort.

Optimized Routing of Intelligent, Mobile Sensors for Dynamic, Data-Driven Sampling

Grant/Contract Number

AFOSR assigned control number. It must begin with "FA9550" or "F49620" or "FA2386".

FA9550-13-1-0162

Principal Investigator Name

The full name of the principal investigator on the grant or contract.

Derek A. Paley

Program Officer

The AFOSR Program Officer currently assigned to the award

Frederica Darema

Reporting Period Start Date

03/27/2013

Reporting Period End Date

06/30/2016

Abstract

The report describes a Dynamic Data-Driven Application Systems (DDDAS) project in which multiple mobile sensors are routed via a data-driven sampling scheme. The long-term goal of this project is to provide a control-theoretic framework to enable intelligent, mobile systems to optimally collect sensor-based observations that yield accurate estimates of unknown processes such as aircraft formation flight and environmental monitoring. The basic research objective is to apply tools from aerospace engineering, specifically nonlinear estimation and control, to design coordinated sampling trajectories that yield the most informative measurements of estimated dynamical and stochastic systems. The technical approach to achieve this objective is to construct a framework for dynamic, data-driven sampling algorithms that (1) maximize the observability of a nonlinear dynamical system subject to time-varying perturbations; and (2) minimize the uncertainty in the estimate of a nonstationary random process that requires nonuniform sampling. The approach incorporates complementary representations of an unknown process: the first uses a deterministic, model-based parametrization, whereas the second uses a low-dimensional statistical description; both approaches apply and enable the DDDAS concept in which measurement data is used to update the model description and the updated model is used to guide subsequent measurements.

FA9550-13-1-0162

Distribution Statement

This is block 12 on the SF298 form.

Distribution A - Approved for Public Release

Explanation for Distribution Statement

If this is not approved for public release, please provide a short explanation. E.g., contains proprietary information.

SF298 Form

Please attach your [SF298](#) form. A blank SF298 can be found [here](#). Please do not password protect or secure the PDF. The maximum file size for an SF298 is 50MB.

[sf0298.pdf](#)

Upload the Report Document. File must be a PDF. Please do not password protect or secure the PDF . The maximum file size for the Report Document is 50MB.

[paley-dddas-final-report.pdf](#)

Upload a Report Document, if any. The maximum file size for the Report Document is 50MB.

Archival Publications (published) during reporting period:

- [1] N. Sydney and D. A. Paley. Multivehicle coverage control for nonstationary spatiotemporal fields. *Automatica*, 50(5):1381–1390, 2014.
- [2] L. DeVries and D. A. Paley. Wake estimation and dynamic control for autonomous aircraft in formation flight. In Proc. AIAA Conf. Guidance, Navigation, and Control, number AIAA-2013-4705, Boston, Massachusetts, August 2013.
- [3] L. DeVries and D. A. Paley. Observability-based optimization of controlled sampling formations for flowfield estimation. AMS Spring Eastern Sectional Meeting, Data Assimilation Session, March 2014.
- [4] D. A. Paley, L. DeVries, and N. Sydney. Data-driven routing of autonomous vehicles for distributed estimation of spatiotemporal fields. Submitted.
- [5] N. Sydney, D. A. Paley, and D. Sofge. Physics-inspired robotic motion planning for cooperative Bayesian target detection. Presented at Robotics Science and Systems 2014, Workshop on Distributed Control and Estimation for Robotic Vehicle Networks, July 2014.
- [6] D. Yeo, N. Sydney, D. A. Paley, and D. Sofge. Onboard flow sensing for downwash detection and avoidance with a small quadrotor helicopter. In Proc. AIAA Guidance, Navigation and Control Conf., number AIAA 2015- 1769, pages 1–11, Orlando, Florida, January 2015.
- [7] N. Sydney, D. A. Paley, and D. Sofge. Physics-inspired motion coordination for information-theoretic target detection using multiple aerial robots. Autonomous Robots, pages 1–11, 2015. DOI: 10.1007/s10514-015-9542-0.
- [8] L.DeVries and D.A.Paley. Wake sensing and estimation for relative-position control of autonomous aircraft in formation flight. *AIAA J. Guidance, Control, and Dynamics*, 39(1):32–41, 2015.
- [9] D. Yeo, N. Sydney, D. A. Paley, and D. Sofge. Onboard flow sensing for downwash avoidance with a small quadrotor helicopter. To appear in *AIAA J. Guidance, Control, and Dynamics*.
- [10] D. A. Paley. Flow sensing and control for aerospace vehicles. Presented at SIAM Conference on Control and Its Applications, Paris, France, 8 August 2015.
- [11] B. Barkley and D. A. Paley. Cooperative Bayesian target detection on a real road network using aerial vehicles. In Proc. Int. Conf. Unmanned Aircraft Systems, Arlington, Virginia, June 2016.

New discoveries, inventions, or patent disclosures:

Do you have any discoveries, inventions, or patent disclosures to report for this period?

Yes

Please describe and include any notable dates

Multi-Hole Probe System for Small UAS Flow Measurements (UMD invention disclosure #PS-2016-015)

Do you plan to pursue a claim for personal or organizational intellectual property?

No

Changes in research objectives (if any):

N/A

Change in AFOSR Program Officer, if any:

N/A

Extensions granted or milestones slipped, if any:

N/A

AFOSR LRIR Number

LRIR Title

Reporting Period

Laboratory Task Manager

Program Officer

Research Objectives

Technical Summary

Funding Summary by Cost Category (by FY, \$K)

	Starting FY	FY+1	FY+2
Salary			
Equipment/Facilities			
Supplies			
Total			

Report Document

Report Document - Text Analysis

Report Document - Text Analysis

Appendix Documents

2. Thank You

E-mail user

Sep 26, 2016 09:41:07 Success: Email Sent to: dpaley@umd.edu